Solvothermal synthesis and Curie temperature of monodispersed barium titanate nanoparticles

Yanping Mao [a], Shaoyu Mao [a,*], Zuo-Guang Ye [a,b,**], Zhaoxiong Xie [a], Lansun Zheng [a]

[a] State Key Laboratory for Physical Chemistry of Solid Surfaces, Department of Chemistry, College of Chemistry and Chemical Engineering, Xiamen University, Xiamen 361005, China
[b] Department of Chemistry and 4D lABS, Simon Fraser University, Burnaby, British Columbia V5A 1S6, Canada

ARTICLE INFO

ABSTRACT

Barium titanate (BaTiO$_3$) nanoparticles with various particle sizes were prepared by a solvothermal method. X-ray powder diffraction (XRPD) patterns show that the as-prepared powders are of pure perovskite BaTiO$_3$. Scanning electron microscopy (SEM) reveals that all the particles of BaTiO$_3$ with different sizes are dispersed homogenously and have uniform size. The room temperature and in situ high temperature XRD analyses indicate that both the proportion of the tetragonal phase and the Curie temperature of BaTiO$_3$ increase with increasing particles size. The effects of the reaction parameters, such as the concentration of reactants, the polarity of solvent, the reaction temperature and the amount of surfactant, on the size, morphology and uniformity of BaTiO$_3$ nanoparticles are studied in detail.

© 2010 Elsevier B.V. All rights reserved.

1. Introduction

Lead-free barium titanate (BaTiO$_3$) has been extensively studied for its environment friendly feature and numerous industrial applications. As a typical ferroelectric material, BaTiO$_3$ has been used in sensors, switches, receivers [1–6], etc. As a microwave dielectric ceramics, BaTiO$_3$ is commonly used in dielectric resonators, microwave integrated circuit substrates, dielectric waveguides, dielectric antenna, attenuator, phase adjustment devices [7–14] and multi-layer ceramic capacitors [15,16]. As the electronic devices continue to be down-sized and integrated with the development of nanotechnology, more and more attention has been focused on the "size effect" which seems to limit the applications of ferroelectric nanoparticles. Therefore, the synthesis and the understanding of the ferroelectricity in BaTiO$_3$ nanoparticles have thus become an urgent task [17]. In general, the ferroelectricity decreases significantly with decreasing grain size, which is the so called "size effect". The ferroelectricity of BaTiO$_3$ nanoparticles disappears when the grain size decreases to about 44 nm according to the calculation by Zhong et al. [18–22]. The grain size effect of BaTiO$_3$ ceramics has been extensively studied since it was first reported in 1954 [23–26]. However, it is difficult to study the size effect of BaTiO$_3$ on nanoscale in the samples prepared by traditional solid state reaction and ceramic processing because the grains generally grow up during sintering.

In order to study the size effect in BaTiO$_3$, nanoparticles with various sizes are needed. As a commonly used solution technique, hydrothermal synthesis provides a special physical and chemical environment for the reaction and crystallization of precursors. Compared to other preparation methods, the particles synthesized by the hydrothermal method are usually integral, uniform and well dispersed. Taking advantage of these merits, in this work BaTiO$_3$ nanoparticles with various sizes from 25 to 500 nm have been prepared by an improved hydrothermal or solvothermal method and characterized by X-ray powder diffraction (XRPD) and scanning electron microscopy (SEM). The reaction parameters and conditions that affect the synthetic results are discussed.

2. Experimental

BaTiO$_3$ nanoparticles of various sizes from 25 to 500 nm were prepared by a solvothermal method at 180–200 °C and the molar ratio of barium ion to titanium ion was maintained 1:1 throughout the synthetic process. The following five different preparation processes were used to synthesize the particles of various sizes. The reactants were sealed in a Teflon-lined stainless steel autoclave and placed in an electric furnace (DHG-9036A, Rongfeng Scientific Instrument Co., Ltd. Shanghai) in each preparation process.

(1) The BaTiO$_3$ nanoparticles of 25 nm size were prepared by reacting 2 mmol barium hydroxide octahydrate (98%, Alfa Aesar) and 0.680 ml titanium (IV) n-butoxide (VERTEC®TNBT, 98 + %, Alfa Aesar) in 15 ml methanol at 180 °C for 24 h. In this process, the barium hydroxide octahydrate was first ground, and then mixed with the titanium (IV) n-butoxide–methanol solution. The mixture was stirred for 10 min before being sealed in the Teflon-lined stainless steel autoclave.

* Corresponding author. Tel.: +86 592 2185667; fax: +86 592 2183047.
** Corresponding author at: State Key Laboratory for Physical Chemistry of Solid Surfaces, Department of Chemistry, College of Chemistry and Chemical Engineering, Xiamen University, 422 Siming South Road, Xiamen 361005, China.
Tel.: +86 592 2185667; fax: +86 592 2183047.
E-mail addresses: symao@xmu.edu.cn (S. Mao), zye@sfu.ca (Z.-G. Ye).
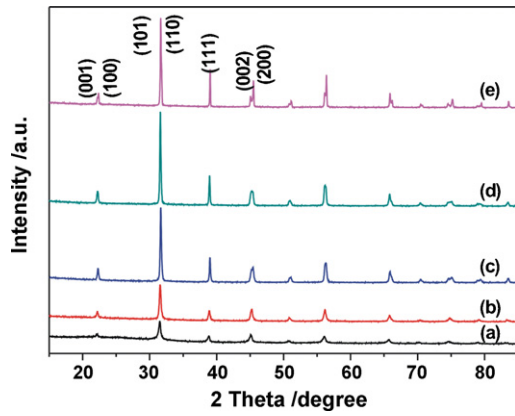
Fig. 1. XRPD patterns of BaTiO$_3$ powders with five typical particle sizes: (a) 25 nm, (b) 50 nm, (c) 80 nm, (d) 150 nm and (e) 500 nm.
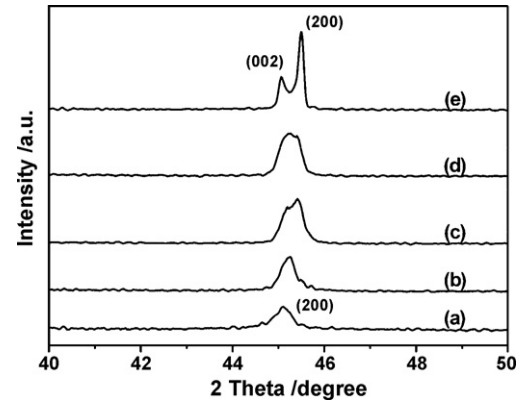

Fig. 2. $(2\,0\,0)_{cub}$ reflection of BaTiO$_3$ powders with various particle sizes: (a) 25 nm, (b) 50 nm, (c) 80 nm, (d) 150 nm and (e) 500 nm.
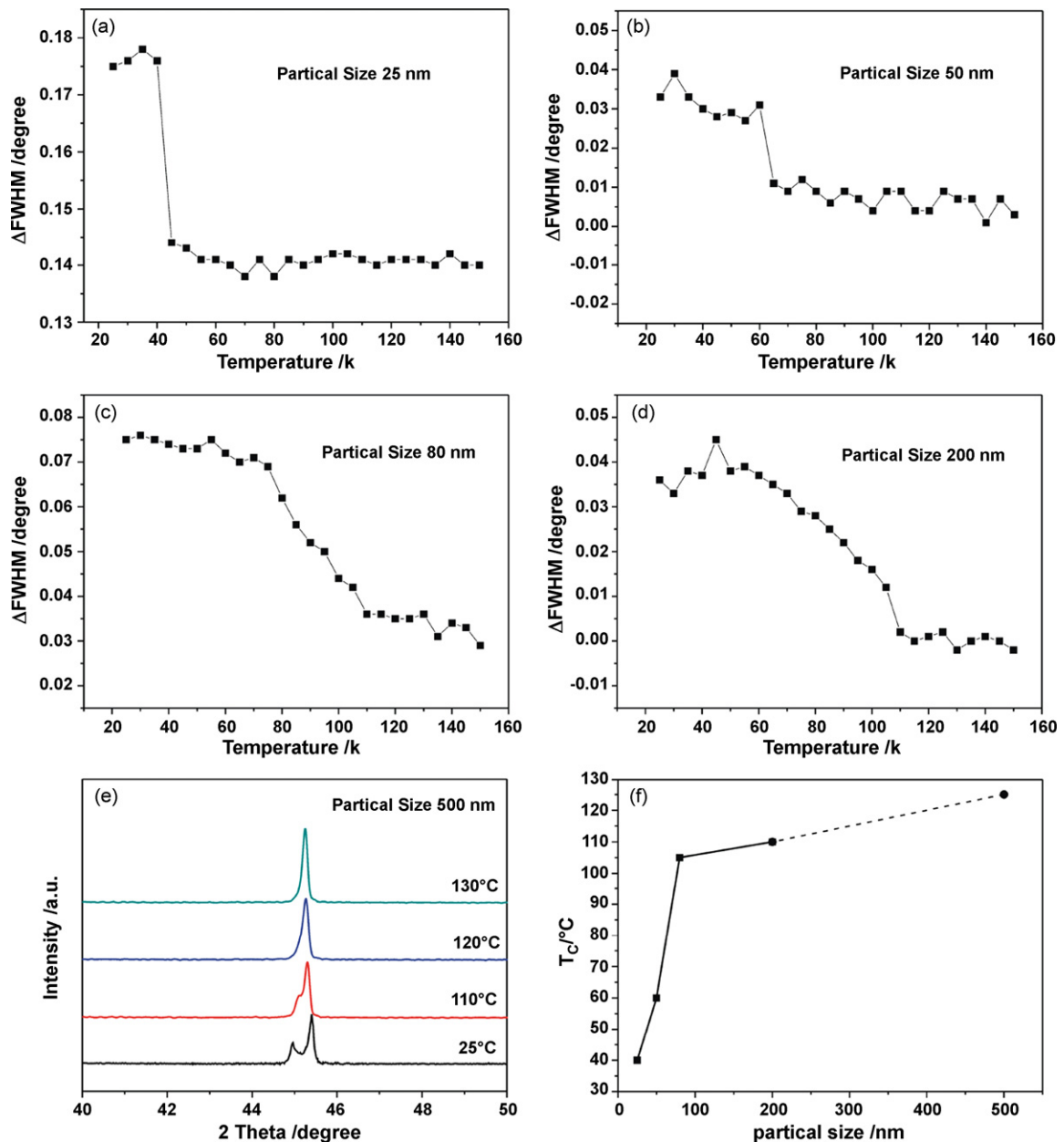

Fig. 3. In situ high temperature XRPD patterns of BaTiO$_3$ samples with various particles sizes: (a) 25 nm, (b) 50 nm, (c) 80 nm, (d) 200 nm and (e) 500 nm. (f) Curie temperature (T_C) as a function of the size of the BaTiO$_3$ nanoparticles.
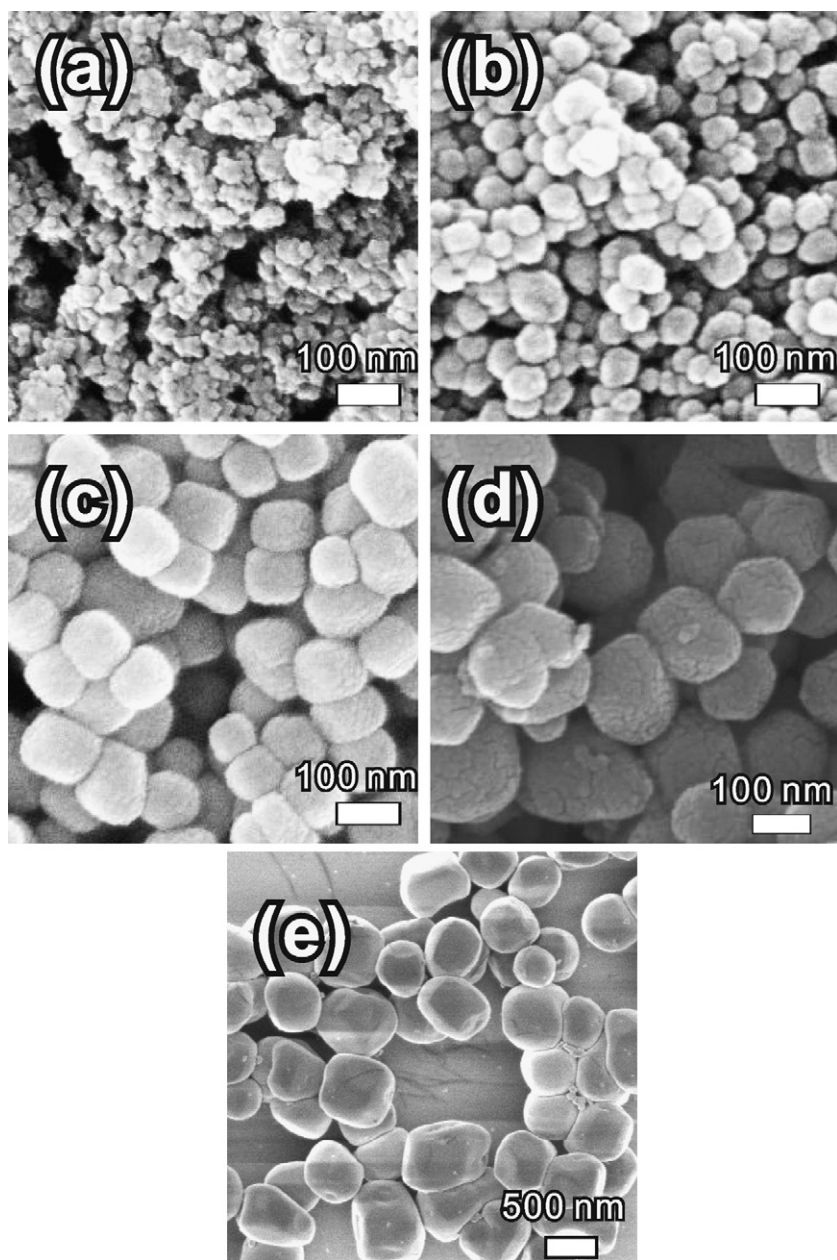
Fig. 4. Scanning electron micrographs of $BaTiO_3$ powders with different particle sizes: (a) 25 nm, (b) 50 nm, (c) 80 nm, (d) 150 nm and (e) 500 nm, corresponding to the five diffraction patterns shown in Fig. 1.
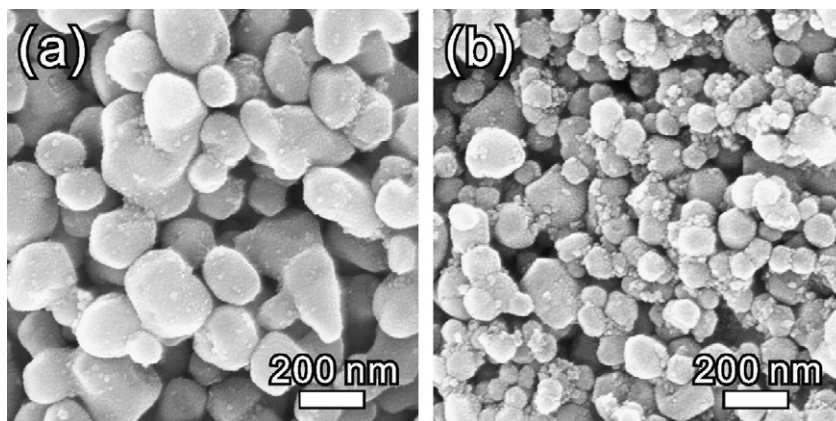

Fig. 5. Scanning electron micrographs of $BaTiO_3$ nanoparticles synthesized using different concentrations of $Ba(OH)_2/H_2O$ and $Ti(OBu)_4/C_6H_{14}$ solutions: (a) 0.20 mol L^{-1} and (b) 1.00 mol L^{-1}.
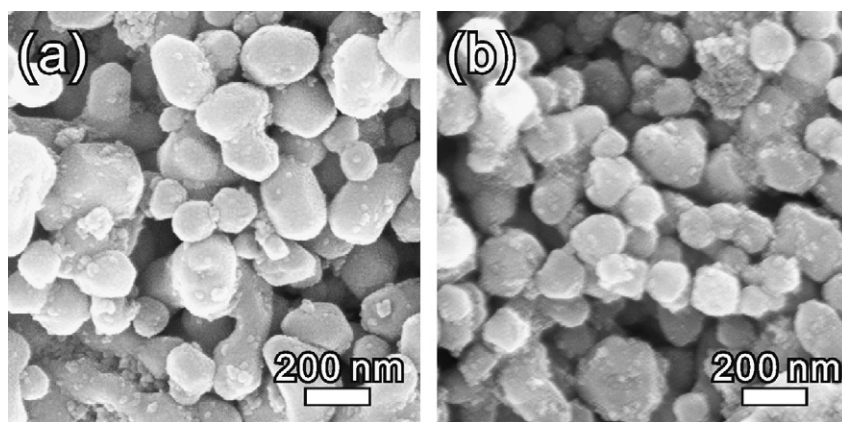
Fig. 6. Scanning electron micrographs of $BaTiO_3$ nanoparticles synthesized with different concentrations of CTAB: (a) 1.00 mmol L^{-1} and (b) 10.00 mmol L^{-1}.

(2) The 50 nm $BaTiO_3$ nanoparticles were synthesized by reacting 2 mmol barium hydroxide octahydrate and 2 mmol titanium dioxide in 35 ml 25% ammonia solution at 200 °C for 24 h. In this process, 2 mmol barium hydroxide octahydrate and 2 mmol titanium dioxide were ground separately before being mixed in a 35 ml 25% ammonia solution. The mixture was stirred for 10 min before being sealed in the Teflon-lined stainless steel autoclave.

(3) The 80 nm $BaTiO_3$ nanoparticles were prepared by reacting 5 mmol barium hydroxide octahydrate and 5 mmol metatitanic acid which was obtained by reacting titanium (IV) chloride in hot NaOH aqueous solution. In this process, 5 mmol ground barium hydroxide octahydrate powder was first put in a beaker, and then 5 mmol metatitanic acid and 15 ml ethanol were added into the beaker successively. The mixture was stirring for 10 min before being sealed in the Teflon-lined stainless steel autoclave which was heated at 180 °C for 24 h.

(4) The $BaTiO_3$ particles with sizes of 100–250 nm were synthesized by reacting 1–5 mmol barium hydroxide octahydrate and 1–5 mmol titanium (IV) n-butoxide in 20 ml n-hexane mixed with deionized water (volume ratio 1:1) for 24 h. In this reaction, 1–5 mmol ground barium hydroxide octahydrate powder was first dissolved in 20 ml deionized water. The solution was then put in the Teflon-lined stainless steel autoclave, in which an equimolar amount of Ti(OBu)$_4$ dissolved in 20 ml hexane was then added. The mixture was heated at 180 °C for 24 h.

(5) The 500 nm $BaTiO_3$ nanoparticles were produced by the following process: 5 mmol barium hydroxide octahydrate, 5 mmol titanium dioxide and 30 ml 20 mol L^{-1} sodium hydroxide solution were mixed and stirred for 10 min before being sealed in the Teflon-lined stainless steel autoclave which was heated at 180 °C for 120 h. It is worth noting that the particle size tends to increase with increasing reaction time, but when the reaction time is beyond a certain period, for example 2 days for 50 nm $BaTiO_3$, the particle size remains stable.

The $BaTiO_3$ powders with various particle sizes were characterized by room temperature X-ray powder diffraction (XRPD). The particle sizes mentioned in this work represent the average particle sizes. Based on the X-ray powder diffraction data, we used the Scherrer formula to calculate the $BaTiO_3$ nanoparticle sizes and their distributions, except for the 500 nm particles which were too big to be calculated using the Scherrer formula. So, we measured the size distribution of the 500 nm particles by scanning electron microscopy. The results from these two analytic techniques
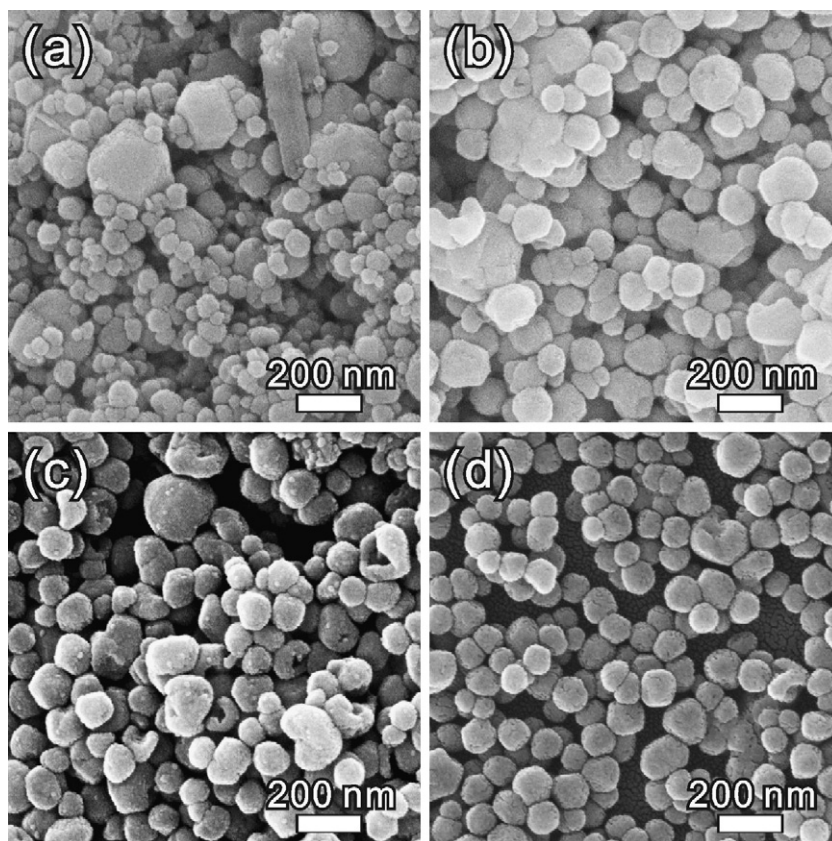

Fig. 7. Scanning electron micrographs of $BaTiO_3$ nanoparticles synthesized using different kinds of solvents: (a) methanol, (b) n-butanol, (c) n-octanol and (d) n-pentane.
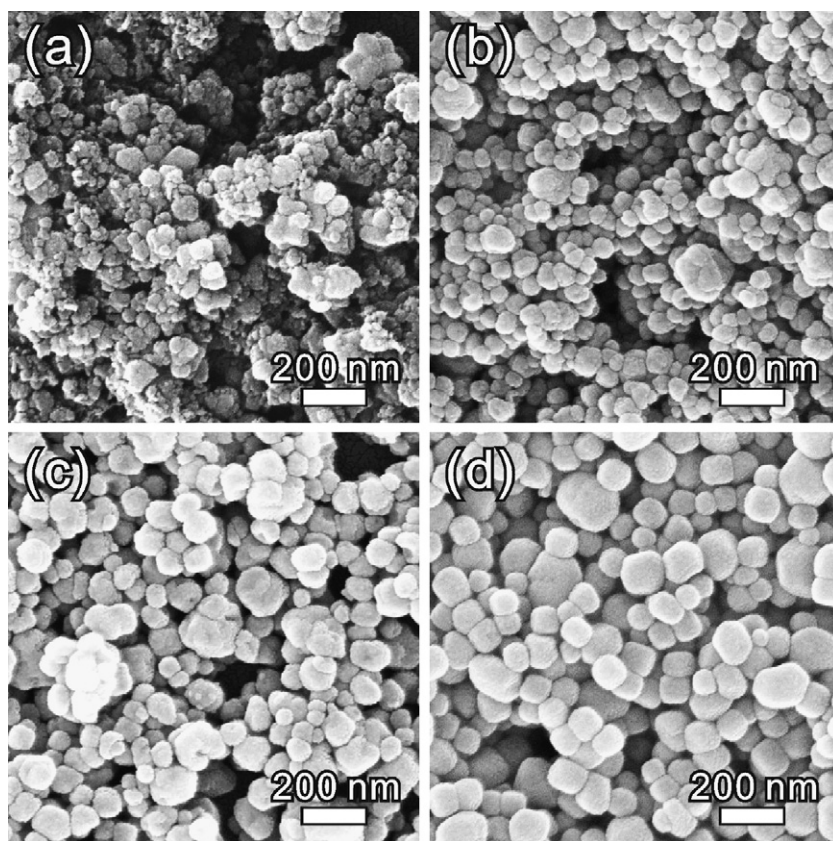
Fig. 8. Scanning electron micrographs of BaTiO₃ nanoparticles synthesized at different temperatures: (a) 150 °C, (b) 170 °C, (c) 180 °C and (d) 200 °C.

are consistent with each other. In order to find the Curie temperature of $BaTiO_3$ particles with various sizes, high temperature X-ray powder diffraction (HTXRPD) experiments were carried out to monitor the structure of the $BaTiO_3$ powders as a function of temperature. The XRPD and HTXRPD patterns were collected in air on a PANalytical X'pert PRO diffractometer with Cu Kα radiation. A PW3050/60 Standard Resolution Goniometer was used in X'pert PRO MPD with vertical and θ–2θ scan mode. Alumina was used as the standard for the calibration of the high temperature stage. A Pt/Rh–13% thermocouple spot-welded to the bottom of the stage was used for measuring the temperature. The samples were 1 mm in thickness and 14 mm in width. The HTXRPD patterns were collected in the 2θ region of 15–85° in continuous mode with a step of 0.0167 in 2θ, at the temperatures ranging from 25 to 150 °C. A heating rate of 4 °C min^{-1} and a soaking time of 8 min were employed. The XRPD profiles were refined using X'Pert High Score program to obtain information on the lattice parameters.

To image the morphology of the particles synthesized and to reveal their size and dispersion, the $BaTiO_3$ powders were examined using scanning electron microscopy (FE-SEM, LEO 1530).

3. Results and discussion

3.1. Structure and morphology of BaTiO₃ nanoparticles

The XRPD patterns obtained from the powders with five typical particle sizes: 25, 50, 80, 150 and 500 nm, are given in Fig. 1. These patterns show that all the samples are of pure perovskite $BaTiO_3$ phase. A small amount of $BaCO_3$ impurity phase was removed by washing in dilute formic acid solution.

In the standard XRPD pattern of $BaTiO_3$, the peak around 45° is indexed with $(2\,0\,0)$ in the cubic phase and it splits into $(0\,0\,2)$ and $(2\,0\,0)$ peaks in the tetragonal phase. The detailed profile of the pseudo-cubic $(2\,0\,0)$ diffraction peak is shown in Fig. 2. The XRPD patterns of the 25 and 50 nm particles reveal a clean cubic symmetry, while the $(2\,0\,0)_{cub}$ peaks of the 80–150 nm particles become broadened and asymmetric, indicating a mixture of cubic and tetragonal phases. The $(2\,0\,0)_{cub}$ peak of the 500 nm parti-

cles exhibits a clear split, indicating a tetragonal symmetry at room temperature. As shown in Fig. 3(a)–(e), the proportion of the cubic phase decreases and that of tetragonal phase increases with increasing particle sizes of $BaTiO_3$ from 25 to 500 nm.

In the standard XRPD pattern of $BaTiO_3$, the peak around $2\theta = 38°$ is indexed to $(1\,1\,1)_{cub}$ in both cubic and tetragonal phases. Since it is difficult to find the Curie temperature of $BaTiO_3$ particles from the XRPD patterns directly, we use the difference between the full-width-at-half-maximum (FWHM) of the pseudo-cubic $(2\,0\,0)$ peak and that of $(1\,1\,1)$ peak, i.e. ΔFWHM, to monitor the structural phase transition in the $BaTiO_3$ nanoparticles. In this way, the peak broadening purely due to the small particle sizes can be eliminated. The values of ΔFWHM as a function of temperature for the $BaTiO_3$ particles of 25–200 nm were shown in Fig. 3(a)–(d). In Fig. 3(a) and (b), the variations of the ΔFWHM of the 25 and 50 nm particles show discontinuous changes at 40 and 65 °C, respectively, which indicate the Curie temperature (T_C) of the $BaTiO_3$ nanoparticles. Therefore, T_C increases from 40 °C for the 25 nm particles, to 65 °C for the 50 nm particles. When the particles size increases to 80 and 200 nm, the changes of ΔFWHM as a function of temperature become more diffuse before reaching a nearly constant value above 110 and 115 °C, respectively, which indicate their respective Curie temperatures. Fig. 3(e) shows the XRPD patterns of the 500 nm $BaTiO_3$ particles recorded at different temperatures. It can be seen that upon heating the split of the $(2\,0\,0)$ peaks disappears at 120 °C, but the $(2\,0\,0)$ peaks are asymmetric. When the temperature reaches 130 °C, the $(2\,0\,0)$ peaks become symmetric, indicating the tetragonal to cubic phase transition at a Curie temperature 120 °C < T_C < 130 °C. Fig. 3(f) shows the variation of the Curie temperatures as a function of the size of the $BaTiO_3$ nanoparticles. The X-ray powder diffraction patterns measured at room temperature before heating and after cooling show no significant changes in ΔFWHM. This indicates that the temperature dependence of

ΔFWHM is reversible and no annealing effect was observed by heating the samples up to 150 °C.

A composite-structural model was used by Wada et al. to explain this size effect of BaTiO$_3$ particles [27]. It includes a gradient lattice strain layer (GLSL) between an inner tetragonal core and a surface cubic layer of BaTiO$_3$ particles. The surface cubic layer is nearly constant (10–15 nm thick). This theory suggests that the crystal structures of the three regions do not depend on the particle sizes, while only the volume fractions of these regions change with the particle size. According to this theory, when the size of BaTiO$_3$ particles varies from 200 to 50 nm, the volume fraction of the tetragonal core decreases, and the jump of ΔFWHM decreases. A minimum jump of ΔFWHM was observed for the particle size of 50 nm (Fig. 3(b)). When the particle size continues to decreases, down to 25 nm for example, a clearer and larger jump was found. This phenomenon is consistent with our previous studies on the size-dependent dielectric property of BaTiO$_3$/PVDF nanocomposites. A minimum of dielectric constant of BaTiO$_3$/PVDF composite with BaTiO$_3$ particle size of 50 nm was observed in that work. This may indicate that the composite-structural model proposed by Wada et al. is suitable only for the particle sizes ranging from 50 to 500 nm. When the particle size decreases to 25 nm, the interface between the tetragonal inner core and the gradient lattice strain layer, as well as the interface between the cubic surface layer and the gradient lattice strain layer become blurred, and thereby the particles present only a GLST (gradient lattice strain layer)-like grain. Upon heating, the structure of the GLST-like nanoparticles transforms immediately into cubic phase, and the ΔFWHM undergoes a sharp drop at T_C. When the size of BaTiO$_3$ particles is of 80–200 nm, the volume fraction of the inner tetragonal core increases. The inner tetragonal core of BaTiO$_3$ particles transforms to the cubic phase gradually with increasing temperature, and once the phase transition is completed, ΔFWHM becomes nearly constant. The volume fraction of the surface cubic layer is small in the 500 nm BaTiO$_3$ particles, and therefore, the (2 0 0) peak exhibits a clear split at room temperature, as shown in Fig. 3(e). When the temperature reaches 130 °C, the (2 0 0) peak shows a symmetric profile, indicating that the Curie temperature of the 500 nm BaTiO$_3$ particles is between 120 and 130 °C.

Fig. 4 shows the SEM micrographs for the five different sizes of particles, corresponding to the five diffraction patterns shown in Fig. 1. It can be seen that all the five batches of BaTiO$_3$ particles have uniform sizes and homogenous dispersions. The particle sizes calculated from the Scherrer formula based on the diffraction patterns match well the sizes revealed by SEM.

3.2. Effects of reaction parameters

In the preparation of BaTiO$_3$ particles with various sizes, it is found that the particle size and its dispersion are related to different solvothermal reaction parameters. In order to study the impact of these parameters, reaction processes 3 and 4 described in Section 2 are selected as examples to illustrate the effects of reaction parameters on the size and its distribution of the BaTiO$_3$ particles so prepared.

3.2.1. Effect of reagent solution concentration

The reagent concentrations of Ba(OH)$_2$/H$_2$O and Ti(OBu)$_4$/C$_6$H$_{14}$ are found to be critical parameters controlling the morphology of the product. The growth process with small reagent concentrations (0.2 mol L^{-1}) yields BaTiO$_3$ of large particle size (200 nm), as illustrated in Fig. 5(a). When the reagent concentrations of Ba(OH)$_2$/H$_2$O and Ti(OBu)$_4$/C$_6$H$_{14}$ solutions are increased to 1.00 mol L^{-1}, the size of BaTiO$_3$ particles decreases to 100 nm and the particles exhibit a more uniform size with a better dispersion, as shown in Fig. 5(b). Therefore, it is demonstrated that a higher reagent concentration

favours initial multiple nucleations due to a higher supersaturation, giving rise to a large number of BaTiO$_3$ particles of smaller size.

3.2.2. Effect of surfactant

It is worth noting that the surfactant has an influence on the morphology of BaTiO$_3$ particles. Surfactant cetyltrimethylammonium bromide (CTAB) was added to the Ba(OH)$_2$/H$_2$O solution instead of pure Ba(OH)$_2$ aqueous solution. The scanning electron micrographs of BaTiO$_3$ nanoparticles synthesized with different concentrations of CTAB, (a) 1.00 mmol L^{-1} and (b) 10.00 mmol L^{-1}, are shown in Fig. 6. It can be seen that the 1.00 mmol L^{-1} CTAB solution has almost no influence on the BaTiO$_3$ particle size, while the 10.00 mmol L^{-1} CTAB solution leads to a smaller average BaTiO$_3$ particle size, from 150 to 100 nm. The BaTiO$_3$ particles size decreases with increasing CTAB solution concentration. We conjecture that small emulsion droplets formed in water/n-hexane two-phase system in a solvothermal environment, and that Ba(OH)$_2$ and Ti(OBu)$_4$ reacted to produce BaTiO$_3$ nanoparticles in the emulsion droplets. The surfactant CTAB reduced the droplet size, leading to BaTiO$_3$ particles of smaller size.

3.2.3. Effect of solvent

The polarity of the solvent is found to be an important parameter affecting the morphology of the BaTiO$_3$ particles. Fig. 7 provides direct information about the typical shape and size of the particles synthesized by the solvents of different polarities, from polar alcohols to non-polar n-pentane. The growth process with polar solvent methanol and n-butanol yields non-uniform particles, as illustrated in Fig. 7(a) and (b). The majority of BaTiO$_3$ particles synthesized by polar methanol is of 60 nm size (the remaining is of 200 nm), the particles synthesized by less polar solvent n-octanol are of 100 nm (Fig. 7(c)), while the particles prepared by the non-polar solvent n-pentane have a size of 80 nm, with the highest uniformity and most homogenous dispersion (Fig. 7(d)). Therefore, the size of the BaTiO$_3$ particles decreases, while the uniformity increases, with the decrease of the polarity of the solvent used. Although further investigations into the effects of solvents on the nucleation and growth of nanoparticles need to be carried out, from the above experimental observations, we can conclude that Ostwald ripening or sequential nucleation tends to occur in polar solvents, while instantaneous nucleation tends to take place in non-polar solvents. Therefore, polar solvents generally lead to a broader distribution of particle sizes.

3.2.4. Effect of reaction temperature

When Ti(OH)$_4$ was prepared and other reaction parameters were kept the same, the reaction temperature is found to play a role in the morphology of the BaTiO$_3$ particles. Fig. 8 shows the growth of BaTiO$_3$ particles prepared at different temperatures: (a) 150 °C, (b) 170 °C, (c) 180 °C and (d) 200 °C. The particles size increases with increasing reaction temperature. A high temperature not only enhances the crystallinity and the growth rate of BaTiO$_3$ nanostructures, but also improves the uniformity of the particle size. In this case, BaTiO$_3$ nanoparticles with pseudo-cubic shape and uniform dimensions are obtained at the highest reaction temperatures of 200 °C. In contrast, at a lower reaction temperature of 150 °C, the reaction proceeds more slowly, giving rise to the BaTiO$_3$ nanoparticles of various sizes.

Compared to the previous work reported by Bocquet et al. on the preparation of BaTiO$_3$ nanoparticles by solvothermal reaction, our synthetic technique represents a simplified and improved preparation process with a single step. By appropriately adjusting the reaction parameters, such as reagent solution concentration, surfactant, solvent, reaction temperature and reaction time, uniform and well dispersed BaTiO$_3$

nanoparticles with various sizes (from 25 to 500 nm) have been synthesized.

4. Conclusions

BaTiO$_3$ nanoparticles with various particle sizes have been prepared by an improved solvothermal method. The particles were of pure perovskite phase, uniform and well dispersed, as proved by means of XRD and SEM. The room temperature and in situ high temperature XRD analyses have revealed that the proportion of tetragonal phase and Curie temperature of BaTiO$_3$ increase with the increasing particle size. The effects of the reaction parameters on the size, morphology and uniformity of the BaTiO$_3$ particles have been studied in detail. It is found that the particle size of BaTiO$_3$ decreases with increasing reactant and surfactant concentrations, the uniformity of the BaTiO$_3$ particles increases with decreasing polarity of the reaction solvent, and finally the crystallinity and the growth rate of BaTiO$_3$ particles increases with increasing reaction temperature. These trends provide useful guidance for the synthesis of BaTiO$_3$ nanoparticles with controlled size, morphology and uniformity.

Acknowledgements

References

[1] G. Arlt, J. Mater. Sci. 25 (1990) 2655.
[2] D. Berlincourt, H.H.A. Krueger, J. Appl. Phys. 30 (1959) (1804).
[3] R.F. Brown, Can. J. Phys. 39 (1961) 741.
[4] W.R. Buessem, L.E. Cross, A.K. Goswami, J. Am. Ceram. Soc. 49 (1966) 36.
[5] B. Jaffe, W.R. Cook Jr., H. Jaffe, Piezoelectric Ceramics, Academic Press, London, New York, 1971.
[6] F. Jona, G. Shirane, Ferroelectrics Crystals, Pergamon Press, New York, 1962.
[7] Z. Li, S.-K. Chan, M.H. Grimsditch, E.S. Zouboulis, J. Appl. Phys. 70 (1991) 7327.
[8] Z. Li, C.M. Foster, X.-H. Dai, X.-Z. Xu, S.-K. Chan, D.J. Lam, J. Appl. Phys. 71 (1992) 4481.
[9] M.E. lines, A.M. Glass, Principles and Applications of Ferroelectrics and Related Materials, Clarendon, Oxford, UK, 1977.
[10] R.E. Newnham, G.R. Ruschau, J. Am. Ceram. Soc. 74 (1991) 463.
[11] R.E. Newnham, S. Trolier-Mckinstry, Apr. MRS Bull. 18 (1993) 27.
[12] K. Uchino, S. Nomura, Ferroelectr. Lett. 44 (1982) 55.
[13] A.Q. Jiang, J.F. Scott, H. Lu, Z. Chen, J. Phys.: Condensed Matter 15 (2003) L305.
[14] C. Basceri, S.K. Streiffer, A.I. Kingon, R. Waser, J. Appl. Phys. 82 (1997) 2497.
[15] L.C. Sengupta, S. Sengupta, IEEE Trans. Ultrason. Ferroelectric Frequency Control 44 (1997) 792.
[16] J.H. Herbert, Ceramic Dielectrics and Capacitors, Gordon and Breach, New York, 1985.
[17] B. Cui, X. Wang, Y.-D. Li, Chem. J. Chin. Univ. 28 (2007) 1.
[18] K. Kinoshita, A. Yamaji, Jpn. J. Appl. Phys. 47 (1976) 371.
[19] G. Arlt, D. Hennings, G. De With, J. Appl. Phys. 58 (1985) 1619.
[20] K. Uchino, E. Sadanaga, T. Hirose, J. Am. Ceram. Soc. 72 (1989) 1555.
[21] M.H. Frey, D.A. Payne, Phys. Rev. B 54 (1996) 3158.
[22] W.L. Zhong, Y.G. Wang, P.L. Zhang, B.D. Qu, Phys. Rev. B 50 (1994) 698.
[23] H. Kniepkamp, W. Heywang, Z. Angew. Math. Phys. 6 (1954) 385.
[24] S. Wada, T. Suzuki, T. Noma, J. Ceram. Soc. Jpn. 104 (1996) 383.
[25] D. McCauley, R.E. Newnham, C.A. Randall, J. Am. Ceram. Soc. 81 (1998) 979.
[26] Z. Zhao, V. Buscaglia, M. Viviani, M.T. Buscaglia, L. Mitoseriu, A. Testino, M. Nygren, M. Johnsson, P. Nanni, Phys. Rev. B 70 (2004) 024107.
[27] T. Hoshina, S. Wada, Y. Kuroiwa, T. Tsurumi, Appl. Phys. Lett. 93 (2008) 192914.